

# SSB Noise Figure Measurements of Frequency Translating Devices

N. Otegi, N. Garmendia, J.M. Collantes, M. Sayed<sup>1</sup>

Electricity and Electronics Department, University of the Basque Country, Apdo. 644, 48080 Bilbao, Spain  
<sup>1</sup>Microwave & MillimeterWave Solutions, Santa Rosa, California, USA

**Abstract** — A complete procedure and formulation for Single-Side-Band (SSB) noise figure characterization of frequency converters are proposed in this paper. The procedure takes into account systematic errors due to mismatch and includes receiver noise calibration. Measurements of three devices with different conversion gain, noise and match characteristics are given. Comparisons of the proposed methodology with several other approximations of the SSB noise figure calculation are also provided.

**Index Terms** — noise figure, noise measurements, mixer characterization.

## I. INTRODUCTION

Noise figure characterization of frequency converters is a complex task that can be affected by different parameters (port matching, conversion at image frequency and idler frequencies...). In addition, there is often confusion and misunderstanding regarding the standard definition of noise figure in frequency translating devices [1]. However, IEEE provides a clear definition for the noise figure at a specific input frequency [2]:

$$F = \frac{N_{out}}{kT_0 G_1} \quad (1)$$

where,  $N_{out}$  is the total noise power per unit bandwidth at the output frequency available at the output port when the noise temperature of its input termination is  $T_0 = 290\text{ K}$  at all frequencies.  $kT_0 G_1$  is the portion of  $N_{out}$  that is engendered at the input frequency by the input termination at temperature  $T_0$ . In the case of a frequency converter,  $G_1$  is the available conversion gain relating the input frequency to the output frequency (considering that in normal operation of the heterodyne system, signal is only present at the input frequency). Thus, the denominator in (1) represents the noise from the input termination which appears in the output via the principal frequency transformation of the device  $G_1$ . This denominator does not include contributions from image-frequency conversion or other idler frequency conversion. It should be noted that this definition does not exclude in  $N_{out}$  any noise generated at image or idler frequencies, but, on the contrary, excludes in the denominator the gain that would correspond to an inexistent signal. In this way, (1) represents the Single Side Band (SSB) noise figure of a frequency converter. It is important to remark that (1) is completely consistent with the fact of considering the noise figure as a

figure of merit that characterizes the degradation of the signal-to-noise ratio from the input to the output of the device.

Typical instruments for noise figure characterization (noise figure analyzers or, more recently, spectrum analyzers) make use of the well-known Y-factor technique to perform the measurements. In the Y-factor technique, the noise figure of the DUT is computed from the ratio  $Y$  of two noise powers measured with a noise source at two temperatures ( $T_h$ ,  $T_c$ , hot and cold temperatures respectively). The noise source is a broadband device that provides extra noise in a wide frequency range when biased in its hot state. Thus, in the case of frequency converters, the obtained result is equivalent to an All-Side-Band (ASB) noise figure in which all the noise contributions of the conversion at image and idler frequencies are present in the denominator ( $G_2, \dots, G_n$ : conversion gains at image and idler frequencies):

$$F_{ASB} = \frac{(T_h/T_0 - 1)}{Y - 1} \equiv \frac{N_{out}}{kT_0 B (G_1 + G_2 + \dots + G_n)} \quad (2)$$

Often, in order to obtain the SSB noise figure from a Y-factor technique the following assumption is made [1]: image conversion is equal to principal conversion ( $G_1 = G_2$ ) and all idler conversions are negligible ( $G_3 = \dots = G_n = 0$ ). Then, SSB noise figure is considered to be simply 3 dB higher than the measured one. Obviously, this assumption will not be satisfied under any conditions and for any frequency translating device. Obtaining a “true” SSB noise figure measurement through a Y-factor technique requires the inclusion of a filter at the input of the device that filters out image and idler frequencies. However, impedance terminations of the mixer input port at image and idler frequencies can have a non negligible influence on the device noise performances [3]. Therefore, if the filter is not required for the device regular operation, some amount of error should be expected in the characterization.

An additional source of error in the standard Y-factor noise figure characterization is related with the mismatch in DUT and measurement path. Since Y-factor only makes use of scalar power measurements, no vector corrections are applied to account for mismatch. However, systematic errors associated to device output mismatch are magnified when the device has loss instead of gain [4], which is the case of most mixers. In addition, poor input match maximizes the error due to changes in the noise source reflection coefficient between its cold and hot temperatures.

In this work a different procedure is proposed to characterize the noise figure of frequency translating devices. Instead of Y-factor, a vector-corrected cold-source technique is used, since this one allows a direct determination of the SSB noise figure. A Spectrum Analyzer (SA) with noise measurement capabilities is used to characterize the noise generated by the DUT with a 50  $\Omega$  termination, at ambient temperature, connected at its input port. The spectrum analyzer and a signal generator serve to measure the principal conversion gain  $G_I$ . A vector corrected formulation is given to compensate for all the mismatch errors. For that, two additional steps are required. First, reflection coefficients at input and output frequencies have to be measured with a Vector Network Analyzer (VNA). Second, a noise calibration of the noise receiver of the SA is also given in order to obtain its gain-bandwidth product and its four noise parameters.

Three diode-based mixers with different characteristics are measured following the proposed procedure. In addition, comparisons with other simplified approaches are analyzed.

## II. SSB NOISE FIGURE CALCULATION

In order to obtain the SSB noise figure defined by (1), the available noise power at the output of the device and the available conversion gain are required.

To compute the available gain, input and output match of the device must be characterized. In fact, the frequency translating device (FTD) can be considered as a cascade of two blocks, one at input frequency and one at output frequency, with a certain  $c_{21}$  conversion gain relating the two blocks. In this sense, the FTD can be seen as an ordinary two-port, whose behavior is ruled by the Local Oscillator (LO) signal and where the conversion from input to output implies also frequency offset (Fig. 1).

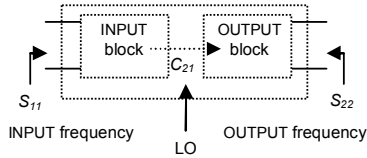


Fig. 1. Simplified scheme of a frequency translating device

Therefore, the available conversion gain from input frequency to output frequency can be expressed as in (3):

$$G_I(\Gamma_s) = \frac{(1-|\Gamma_s|^2)}{|1-\Gamma_s s_{11}|^2} |c_{21}|^2 \frac{1}{(1-|\Gamma_{out}|^2)} \quad (3)$$

where  $\Gamma_s$  is the source reflection coefficient and  $\Gamma_{out}$  is the output reflection coefficient of the FTD. It is important to note that  $s_{11}$  and  $\Gamma_{out}$  must be obtained under operating conditions, i.e. with the LO power at its operating level, to correctly describe the device behavior. Besides, it should be reminded that  $\Gamma_s$  and  $s_{11}$  are measured at input frequency, while  $\Gamma_{out}$  must be characterized at output frequency.  $|c_{21}|^2$  can be

obtained by means of a SA and a signal generator. For that, two noise power measurements are performed:  $P_1$ , with the generator directly connected to the SA and  $P_2$ , which is the power delivered by the device to the SA. From these measurements  $|c_{21}|^2$  can be calculated as,

$$|c_{21}|^2 = \frac{P_2}{P_1} \frac{(1-|\Gamma_{SA\_Fin}|^2)}{(1-|\Gamma_{SA\_Fout}|^2)} \frac{|1-\Gamma_{gen} s_{11}|^2 |1-\Gamma_{out} \Gamma_{SA\_Fout}|^2}{|1-\Gamma_{gen} \Gamma_{SA\_Fin}|^2} \quad (4)$$

where  $\Gamma_{gen}$  is the reflection coefficient of the generator and  $\Gamma_{SA\_Fin}$  and  $\Gamma_{SA\_Fout}$  are the input reflection coefficients of the SA at input and output frequencies, respectively. With typical signal generator and SA match characteristics, (5) can be a fair approximation of the available conversion gain.

$$G_I \approx \frac{(1-|\Gamma_s|^2) P_2}{|1-\Gamma_s s_{11}|^2 P_1 (1-|\Gamma_{out}|^2)} \quad (5)$$

Once device gain is characterized, the noise figure is computed from a unique noise power measurement of the FTD, in the standard manner of cold-source techniques. The noise power is measured, in our case, with the noise capabilities provided by the SA. For that, a 50  $\Omega$  load at ambient temperature is connected at the input of the device.

The noise contribution of the noise receiver of the SA must be eliminated applying the second stage correction. Using straight forward algebra, the SSB noise figure of the device defined by (1) can be obtained from (6).

$$F_{SSB} = \frac{N_{meas}}{kT_0 B G_{rec} MM(\Gamma_{out}) G_I} \quad (6)$$

$$\frac{(T_c - T_0) (G_1 + G_2 + \dots + G_n)}{T_0 G_1} - \frac{F_{rec}(\Gamma_{out}) - 1}{G_1}$$

where  $N_{meas}$  is the measured noise power,  $kBG_{rec}$  the gain-bandwidth product of the SA noise receiver and  $F_{rec}$  its noise figure.  $MM(\Gamma_{out})$  is a mismatch factor between device and SA:

$$MM(\Gamma_{out}) = \frac{1-|\Gamma_{out}|^2}{|1-s_{11\_rec} \cdot \Gamma_{out}|^2} \quad (7)$$

with  $s_{11\_rec}$  the input reflection coefficient of the SA noise receiver at output frequency.

Equation (6) is cumbersome since it includes conversion gains at image and idler frequencies ( $G_2, \dots, G_n$ ). However, in most cases, ambient temperature  $T_c$  can be approximated to reference temperature  $T_0$ . In this case, the SSB noise figure can be obtained from:

$$F_{SSB} = \frac{N_{meas}}{kT_0 B G_{rec} MM(\Gamma_{out}) G_I} - \frac{F_{rec}(\Gamma_{out}) - 1}{G_1} \quad (8)$$

The  $kBG_{rec}$  term is computed in a previous calibration stage, in which a standard noise source is connected to the SA and two power measurements (cold and hot states) are performed,  $N_{c\_rec}$  and  $N_{h\_rec}$ .

$$kBG_{rec} = \frac{N_{h\_rec} - N_{c\_rec}}{T_2 - T_1} \quad (9)$$

$$T_2 = MM(\Gamma_{s\_h})(F_{rec}(\Gamma_{s\_h})T_0 + (T_h - T_0))$$

$$T_1 = MM(\Gamma_{s\_c})(F_{rec}(\Gamma_{s\_c})T_0 + (T_c - T_0))$$

being  $\Gamma_{s\_c}$ ,  $\Gamma_{s\_h}$  the reflection coefficients of the noise source in its cold and hot states, respectively. Finally, the dependence of the noise figure of the SA noise receiver on its source reflection coefficient  $\Gamma$  through four noise parameters has to be determined:

$$F_{rec}(\Gamma) = F_{min} + 4 \frac{R_n}{Z_0} \frac{|\Gamma - \Gamma_{opt}|^2}{|1 + \Gamma_{opt}|^2 (1 - |\Gamma|^2)} \quad (10)$$

This is a crucial step that cannot be ignored. Neglecting this dependence in devices with low gain and mediocre match (as could be the case of some mixers) leads to significant errors in the noise figure calculation, as shown in [4].

Here, a noise calibration procedure originally developed for vector network analyzers [5] is applied to obtain the four noise parameters  $F_{min}$ ,  $R_n$  and  $\Gamma_{out}$  of the SA noise receiver. Proceeding as in [5], the dependence of the second stage correction with source reflection coefficient is concentrated in the following term:

$$I = C_1 + C_2 |\Gamma|^2 + C_3 |\Gamma| \cos(\angle \Gamma - C_4) \quad (11)$$

where  $C_1$ ,  $C_2$ ,  $C_3$  and  $C_4$  are four equivalent noise parameters that can be analytically calculated from the measurement of four known passive loads. Then the classical noise parameters can be deduced from:

$$F_{min} = 1 - \left( C_2 + \frac{C_3}{2|\Gamma_{opt}|} \right) ; \quad R_n = \frac{-C_3 Z_0}{8|\Gamma_{opt}|} (1 + |\Gamma_{opt}|^2) \quad (12)$$

$$|\Gamma_{opt}|^2 + 2 \frac{(C_1 + C_2)}{C_3} |\Gamma_{opt}| + 1 = 0 ; \quad \angle \Gamma_{opt} = -C_4$$

where  $Z_0$  is the characteristic impedance.

This noise calibration procedure avoids the use of typical tuners and optimization processes, which may be excessively cumbersome and time-consuming.

### III. MEASUREMENT RESULTS

Measurement results of three diode-based mixers, with different gain and match characteristics, are given in this section. The three mixers have the same IF frequency. The measurement setup makes use of a SA, a VNA, a noise source and two signal generators in order to compute necessary gain, mismatch and noise powers as required by the procedure described in section II. The characterization is performed versus LO power since the noise generated by a diode-based mixer can be affected by this one [6]. Measurement temperature  $T_c$  can be realistically approximated to  $T_0$ .

In the following we will label  $F_{CS\_VECTOR}$  the vector-corrected cold-source procedure defined by (8). This approach has been applied to obtain the SSB noise figure of the three mixers under study. In addition, results have been compared to three different approximations of the SSB noise figure: One Y-Factor based ( $F_{YF+3}$ ), and two cold-source based approximations with lower level of corrections ( $F_{CS\_SCALAR}$  and  $F_{CS\_MM\_CORR}$ ).

-  $F_{YF+3}$ : This approximation estimates the SSB noise figure by adding 3 dB to the result obtained from a standard Y-Factor measurement, (13). In this approach only scalar measurements are performed, therefore, neither mismatch corrections nor noise parameter calibration are included. Parameters of the second stage correction (8) are approximated by  $F_{rec}(\Gamma_s)$  and all-side-band insertion gain  $G_{ins}$ . These are calculated from the hot and cold measurements ( $N_{h\_rec}$ ,  $N_{c\_rec}$ ) performed with the noise source directly connected to the receiver.

$$F_{YF+3} = \left( \frac{(T_h/T_0 - 1)}{N_{h\_meas}/N_{c\_meas} - 1} - \frac{F_{rec}(\Gamma_s) - 1}{G_{ins}} \right) (dB) + 3 \quad (13)$$

$$G_{ins} = \frac{N_{h\_meas} - N_{c\_meas}}{N_{h\_rec} - N_{c\_rec}} \quad (14)$$

$N_{h\_meas}$  and  $N_{c\_meas}$  are the hot and cold noise powers measured during the DUT characterization.

-  $F_{CS\_SCALAR}$ : this approximation, as shown in (15), represents a scalar version of (8). Available conversion gain is substituted by the insertion gain of the principal conversion,  $G_{Iins} = P_2/P_1$ .  $MM(\Gamma_{out}) = MM(\Gamma_{s\_h}) = MM(\Gamma_{s\_c}) = 1$  and  $\Gamma_{s\_c} = \Gamma_{s\_h} = \Gamma_s$  are considered in (8) and (9). The noise figure of the receiver is again approximated by  $F_{rec}(\Gamma_s)$  since no noise parameter calibration is taken into account.

$$F_{CS\_SCALAR} = \frac{N_{meas}}{kT_0 BG_{rec} G_{Iins}} - \frac{F_{rec}(\Gamma_s) - 1}{G_{Iins}} \quad (15)$$

-  $F_{CS\_MM\_CORR}$ : this approximation adds all the corrections to  $F_{CS\_SCALAR}$  except for the calibration to get the four noise parameters of the SA noise receiver. Thus, the only difference between this approach and the proposed  $F_{CS\_VECTOR}$  is the use of  $F_{rec}(\Gamma_s)$  instead of  $F_{rec}(\Gamma_{out})$  in (8).

Fig. 2 shows the results obtained with the first mixer, *Mix1* (RF = 2 GHz, LO = 3 GHz, IF = 1 GHz). *Mix1* can be seen as a good test device in our case: it presents equal conversion loss for principal and image frequencies and conversions from idler-frequencies are negligible ( $G_1 \approx G_2$ ,  $G_3 \approx \dots \approx G_n \approx 0$ ). In addition, output return loss is better than 10 dB in all the analyzed range. As it could be expected,  $F_{CS\_VECTOR}$  and all the approximations  $F_{YF+3}$ ,  $F_{CS\_SCALAR}$ ,  $F_{CS\_MM\_CORR}$  lead to comparable results. It can be observed that, in this case,  $F_{YF+3}$  provides a good approximation of the SSB noise figure, as expected from the conversion properties of the device. Besides, it is shown that neither vector corrections nor noise calibration are necessary, due to the good match of *Mix1*.

The second mixer *Mix2* (RF = 1.3 GHz, LO = 0.3 GHz, IF = 1 GHz) is now considered. In this case, ( $G_2 + G_3 + \dots + G_n$ ) is larger than  $G_1$  in all of the measurement range, while output match is better than 10 dB. Results plotted in Fig. 3 show that  $F_{YF+3}$  underestimates the SSB noise figure. This is again consistent with the conversion loss characteristics of *Mix2*. On the contrary, the two cold-source approximations,  $F_{CS\_SCALAR}$  and  $F_{CS\_MM\_CORR}$ , provide identical results to  $F_{CS\_VECTOR}$ , due to the good output match of *Mix2*. Therefore,  $F_{CS\_SCALAR}$  can be a judicious approach for obtaining the SSB noise figure of mixers with fair match characteristics.

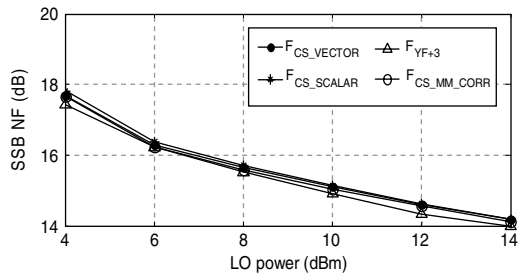


Fig. 2. SSB noise figure characterization of *Mix1* vs. LO power.

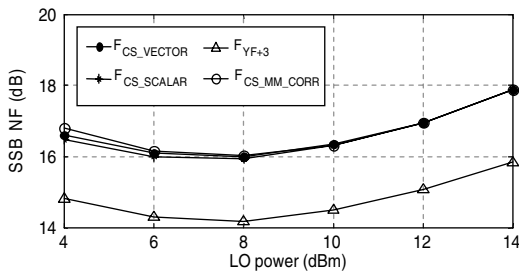


Fig. 3. SSB noise figure characterization of *Mix2* vs. LO power.

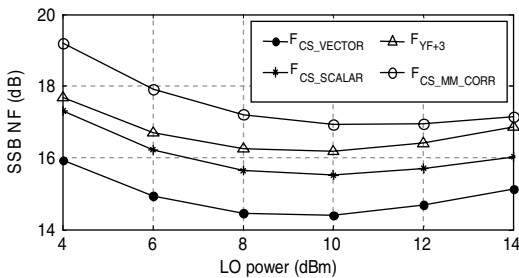


Fig. 4. SSB noise figure characterization of *Mix3* vs. LO power.

Finally, Fig. 4 shows the measurement results for the third case under analysis, *Mix3* (RF = 2 GHz, LO = 3 GHz, IF = 1 GHz). This device, in addition to having different principal and image conversion losses, is poorly matched at the output port, as shown in Fig. 5.

As it can be observed in Fig. 4, four different responses have been obtained. The error associated to  $F_{YF+3}$  has increased from *Mix2*, due to the poor output match. For the same reason,  $F_{CS\_SCALAR}$  cannot provide an accurate result.

Finally, it should be noted the highest error given by  $F_{CS\_MM\_CORR}$ , confirming that mismatch corrections require a receiver noise calibration to be rigorous and efficient [4].

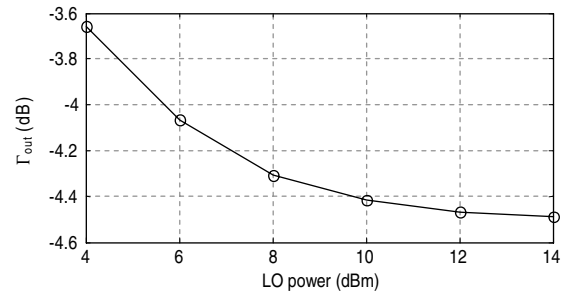


Fig. 5. Output reflection coefficient of *Mix3* vs. LO power.

#### IV. CONCLUSION

A vector-corrected cold-source methodology and formulation are given to characterize the SSB noise figure of frequency translating devices. Mismatch corrections and receiver noise calibration are included in the approach. Three diode-based mixers with different characteristics have been measured following the proposed procedure. Measurement results have been compared with those from other approximations of the SSB noise figure calculation. Comparison results served to evidence which approaches and approximations are judicious depending on device gain and match characteristics, or, on the contrary, when the complete SSB formulation is essentially required.

#### ACKNOWLEDGEMENT

The authors wish to acknowledge Agilent Technologies for their support. This work has been funded by Spanish Commission of Science and Technology (TIC2003-04453).

#### REFERENCES

- [1] S. A. Maas, *Noise in Linear and Nonlinear Circuits*, Artech House, Norwood, MA, 2005
- [2] IRE Subcommittee 7.9 on Noise, "Description of the Noise Performance of Amplifiers and Receiving Systems," *Proc. IEEE*, vol. 51, pp. 436-442, 1963.
- [3] S. A. Maas, *Microwave Mixers, Second Edition*, Artech House, Norwood, MA, 1992
- [4] J. M. Collantes, R.D. Pollard, M. Sayed, "Effects of DUT Mismatch on the Noise Figure Characterization: A Comparative Analysis of Two Y-Factor Techniques," *IEEE Trans. Inst& Meas*, vol. 51, no. 6, December 2002, pp. 1150-1156.
- [5] N. Otegi, J. M. Collantes, M. Sayed, "Calibrated Noise Figure Measurements in Vector Network Analyser," *Electronic Letters*, vol. 41, Issue 18, September 2005, pp. 999-1000
- [6] G. M. Hegazi, A. Jelenski, K.S. Yngvesson, "Limitations of Microwave and Millimeter-Wave Mixers Due to Excess Noise," *IEEE Trans. on MTT*, Vol. 33, N. 12, Dec. 1985, pp. 1404-1409

# Transient Analysis of Pulse Propagation on Planar Ultra-wideband Antenna by Using Transient Electrooptic Near-field Mapping System

Kyoung-Hwan Oh and Jong-In Song

Department of Information and Communications, GIST  
1 Oryong-dong, Buk-gu, Gwangju, Korea 500-712, jisong@gist.ac.kr

**Abstract** — Transient analysis of pulse propagation on a coplanar waveguide (CPW)-fed rectangular slot antenna for ultra-wideband (UWB) communication system application was performed using a transient electrooptic near-field mapping system. Details of short electrical pulse propagation and reflection in the UWB antenna were characterized. The system was very effective in characterizing transient behavior of short electrical pulses in the UWB antenna.

**Index Terms** — Electrooptic measurements, near-field, pulse propagation, transient analysis, UWB antenna.

## I. INTRODUCTION

Ultra-wideband (UWB) communications have received worldwide attention since the allocation of the 3.1~10.6 GHz frequency range by the Federal Communications Commission (FCC) in Feb., 2002 [1], [2]. Antenna is one of key components for UWB communication systems and various types of antenna for UWB application have been proposed [3], [4]. In a narrow-band system, frequency-domain parameters such as return loss, gain, and far-field radiation patterns at the specific operating frequency, are enough to evaluate an antenna performance. However, in a UWB communication system, above-mentioned parameters do not provide enough information for antenna performance over the UWB band. Even with the parameters covering the entire UWB band, it is still difficult to identify whether an antenna is suitable for UWB communications. UWB communication systems deal with generation and transmission of short electric pulses in the order of pico-seconds. These pulses have a broad bandwidth covering the FCC frequency range (3.1~10.6 GHz). Therefore, instead of using the frequency-domain parameters, UWB antennas should be investigated from a different perspective. New characterization approaches of UWB antennas that can provide transient analysis in the time-domain have been proposed [5]-[8]. However, those approaches reported only showed temporal shape of electrical pulses by using an oscilloscope. Recently, a transient electrooptic near-field mapping system, which can provide actual near-field distributions of a planar antenna structure, was successfully demonstrated for characterizing transient near-field patterns of planar passive microwave circuits [9]. This transient electrooptic near-field mapping system can provide information of propagation and

internal reflection of short electric pulses in UWB antennas in detail.

In this paper, transient analysis of short pulse propagation in a CPW-fed rectangular slot antenna is demonstrated by using transient electrooptic near-field mapping system. The system could visually show the transient behavior of short electrical pulse in the UWB antenna.

## II. ANTENNA STRUCTURE

Planar-type antennas have the advantages including compact size and ease of integration with transceiver circuits. A CPW-fed rectangular slot antenna proposed by R. Chair, et al. [10] for UWB antenna was fabricated. Figure 1 shows the fabricated UWB antenna. The slot is etched at the center of a 60 mm × 60 mm ground plane. The substrate (RO4003) has the dielectric constant and thickness of 3.38 and 0.5 mm, respectively. The rectangular slot has the width and length of 36 mm and 20.6 mm, respectively. A 50 Ω coplanar waveguide (slot width of 0.15-mm and center conductor width of 1.8 mm) was used for feeding the antenna. The U-shaped tuning stub embedded within the slot terminates the CPW feed. Dimension of the stub was 16 mm along x-direction and 10 mm in z-direction. Fig. 2 shows simulated and measured scattering parameters of the fabricated UWB antenna which covers the FCC frequency range (3.1~10.6 GHz).

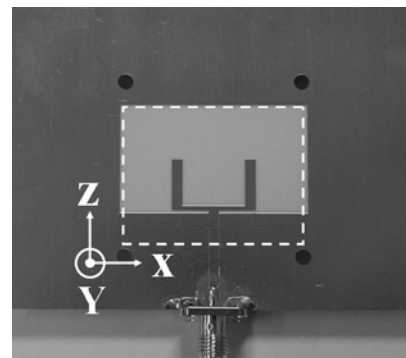


Fig. 1. Fabricated UWB antenna. The dotted area (30 mm × 16 mm)